Chemical Science

ROYAL SOCIETY OF CHEMISTRY

EDGE ARTICLE

View Article Online
View Journal | View Issue

Cite this: *Chem. Sci.*, 2023, **14**, 533

All publication charges for this article have been paid for by the Royal Society of Chemistry

Dative B←N bonds based crystalline organic framework with permanent porosity for acetylene storage and separation†

Weize Wang,‡[a] Linxia Wang,‡[a] Fei Du,[a] Gang-Ding Wang,[b] Lei Hou,*[b] Zhonghua Zhu,[c] Bo Liu*[a] and Yao-Yu Wang[b]

Received 1st November 2022
Accepted 2nd December 2022

DOI: 10.1039/d2sc06016g

rsc.li/chemical-science

The utilization of dative B←N bonds for the creation of crystalline organic framework (BNOF) has increasingly received intensive interest; however, the shortage of permanent porosity is an obstacle that must be overcome to guarantee their application as porous materials. Here, we report the first microporous crystalline framework, BNOF-1, that is assembled through sole monomers, which can be scalably synthesized by the cheap 4-pyridine boronic acid. The 2D networks of BNOF-1 were stacked in parallel to generate a highly porous supramolecular open framework, which possessed not only the highest BET surface area of 1345 $m^2\ g^{-1}$ amongst all of the BNOFs but also features a record-high uptake of C_2H_2 and CO_2 in covalent organic framework (COF) materials to date. Dynamic breakthrough experiments demonstrated that BNOF-1 material can efficiently separate C_2H_2/CO_2 mixtures. In addition, the network can be regenerated in organic solvents with no loss in performance, making its solution processable. We believe that BNOF-1 would greatly diversify the reticular chemistry and open new avenues for the application of BNOFs.

Introduction

Since the first crystalline porous materials were reported in the late 1980s and early 1990s, they have provided an ideal platform for a deep understanding of the structure–performance relationships of materials due to their clear and adjustable structures and controllable properties.[1–3] Metal–organic frameworks (MOFs)[4–6] and covalent organic frameworks (COFs)[7–9] are the most representative of crystalline porous materials, and thus, they are known for their impressive material properties. However, insolubility and poor processability are the limitations of MOF and COF materials, which are related to the inherent strong bonding interactions (coordination/covalent bonds) used to aggregate their building blocks.[10,11] Relatively weak intermolecular supramolecular interactions permit the framework to readily dissolve and regenerate in solvents, endowing the materials with processability to a certain extent.[12–14] Various supramolecular interactions, such as hydrogen bonds,[15,16] halogen bonds,[17,18] and π–π interactions[19] play important roles in producing crystalline supramolecular frameworks. However, the stability of these frameworks is usually not enough, for instance, the removal of lattice molecules often results in framework collapse.[20–22] The few supramolecular networks, which show extrinsic porosity, are mostly based on hydrogen bonds.[23–25] In addition, the large-scale and industrial usage of such materials is still difficult owing to prohibitive production costs.[26–29]

Dative boron–nitrogen bonds (B←N bonds) are very unique in having a strong covalent character, directionality, and reversible nature.[30–32] The utilization of dative B←N bonds in structural supramolecular chemistry has become increasingly popular in recent years.[33–35] Since Kay Severin pioneered the synthesis of the first crystalline organic framework based on the B←N bonds (BNOF) by using triboronate esters and bipyridyl ligands in 2011,[36] other 1D and 2D crystalline BNOFs have been designed and synthesized by combining polytopic N-donor ligands with polyboronate esters.[37–39] It is now known that the robustness of B←N bonds is significantly dependent upon the steric and electronic properties of the interacting components,[33,40] as these properties can prevent the sensitive boronate ester moieties from hydrolyzing.[41–43] Thus B←N bonds stabilize

[a]*College of Chemistry & Pharmacy, Northwest A&F University, Yangling 712100, P. R. China. E-mail: chemliubo@nwsuaf.edu.cn*

[b]*Key Laboratory of Synthetic and Natural Functional Molecule of the Ministry of Education, Xi'an Key Laboratory of Functional Supramolecular Structure and Materials, College of Chemistry & Materials Science, Northwest University, Xi'an 710127, P. R. China. E-mail: lhou2009@nwu.edu.cn*

[c]*School of Chemical Engineering, The University of Queensland, Brisbane, 4072, Australia*

† Electronic supplementary information (ESI) available: Experimental methods, PXRD analysis, TGA curves, additional adsorption isotherms, calculation adsorption selectivity and heat, IR spectra, comparison of adsorption performances and BET, X-ray crystallography details and other data. CCDC 2207247. For ESI and crystallographic data in CIF or other electronic format see DOI: https://doi.org/10.1039/d2sc06016g

‡ These authors have contributed equally to this work.

the resulting organic frameworks. In 2019, Severin's group explored the porosity of BNOFs with sheet-like structures by combining tetrahedral borates with bent diimidazole ligands.[44] However, because these BNOFs exhibit an amorphous state after activation, the reported specific surface area is low (≤314 $m^2 g^{-1}$). The synthesis of BNOFs with permanent porosity is still in the initial stages.

When the dative B←N bond is formed, the Lewis basic N-donor strut is of a monodentate fashion; the configuration of the B atom is converted from trigonal-planar (sp^2) to tetrahedral geometry (sp^3), therefore BNOFs can be controlled and assembled.[45–47] Previously reported the synthesis of supramolecular assemblies based on dative B←N bonds usually included two steps: (i) boric acid condensation with diols and/or self-condensation to form borate esters; (ii) adduct formation of borate esters with N-donor ligand (Scheme 1a and b).[37,38] It was found that the formation of borate esters often increases the complexity of the monomers, leading to more flexible linkers, and forming unstable or interpenetrated frameworks with low void space.[44,48] In contrast, the one-step reaction utilizing a rigid single component not only simplifies the formation procedures but also helps avoid by-products.[49,50] Therefore, the single bifunctional component may be a promising alternative to building BNOFs. This strategy has however only rarely been studied.[31] In this work, we employed an easily obtained and cheap bifunctional monomer, 4-pyridine boronic acid (PBA), to construct microporous BNOFs (Scheme 1c). It can be speculated that a 0D macrocyclic multimer could be formed through bridging pyridine, once boronic acid is condensed into a boroxine ring (B_3O_3). Nevertheless, isoreticular expansion needs to connect two B atoms in a stereoscopic configuration on the boroxine (one boroxine cannot exist with three tetrahedral B atoms due to the steric hindrance effect[51]). As we expected, a 2D crystalline B←N organic framework, BNOF-1, was successfully synthesized by PBA in one step, which is the first BNOF with permanent porosity based on the sole monomer. BNOF-1 can be easily prepared in large amounts and possesses the highest specific surface area compared to previous BNOFs. It also establishes a new benchmark organic framework material for C_2H_2 storage. According to the breakthrough curve, the high dynamic C_2H_2 productivity and selectivity allow BNOF-1 to be potentially applied to the separation of C_2H_2/CO_2 mixtures under actual conditions.

Results and discussion

Crystal structure

Colourless rhombic single crystals of BNOF-1 were obtained under a solvothermal reaction by heating PBA in a mixture of *N*-methylformamide (NMF), MeCN, and HCOOH at 120 °C for 12 h. The single-crystal structure shows that BNOF-1 crystallizes in the orthorhombic space group *Pmmn*. Three PBAs were condensed into a boroxine after removing trimolecular water, and the other two PBAs coordinated with two B atoms in the tetrahedral configuration on the boroxine through dative B←N bonds (Scheme 1c). The B–N bond length of 1.627 Å is similar to the previously reported values.[40,47,52] Every boroxine is connected to four bridged pyridines in the *trans* conformation and one coplanar pyridine (Fig. 1a); the 4-c boroxine node is further extended to construct a 2D layer (Fig. 1b) with **sra** topology. From the *a*-axis, these layers are stacked and overlapped to give rise to a supramolecular framework through weak intermolecular forces, with an interlayer distance of about 3.7 Å (Fig. 1c). A square 1D open channel of ~9.0 × 9.6 $Å^2$ is formed along the *c* direction (Fig. 1b and d), with accessible free voids covering 49.0%. The end-capped pyridines were staggered and modified on the upper and lower surfaces of the layers (Fig. 1c).

Stability

The crystalline phase was characterized by powder X-ray diffraction (PXRD) that shows sharp and strong peaks at 2θ equaling 8.1 and 12.0° for synthesized crystals of BNOF-1

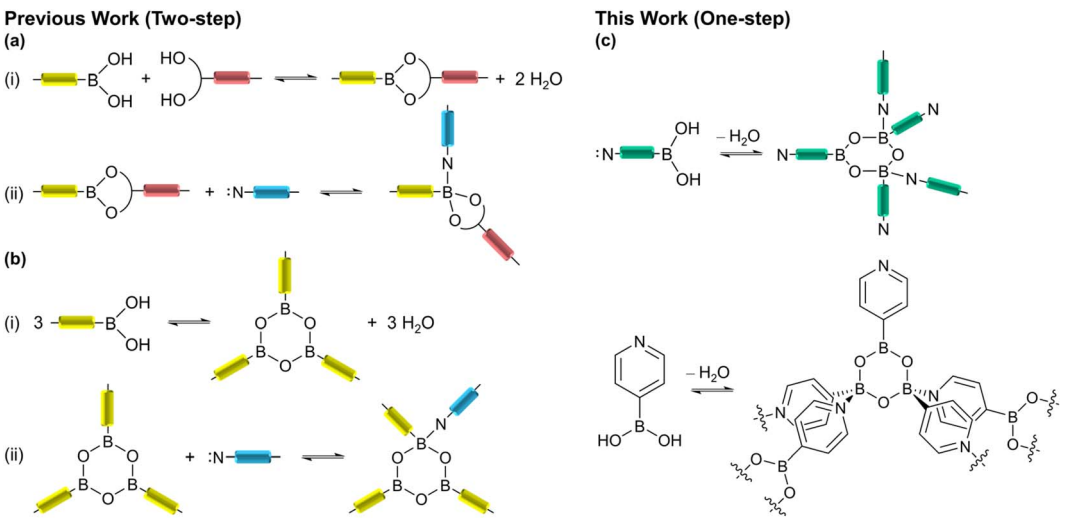

Scheme 1 (a) and (b) Supramolecular assemblies based on dative B←N bonds that were synthesized in two steps according to previous reports. (c) The incorporated bifunctional monomer used in this work and a fragment of the 2D network in BNOF-1.

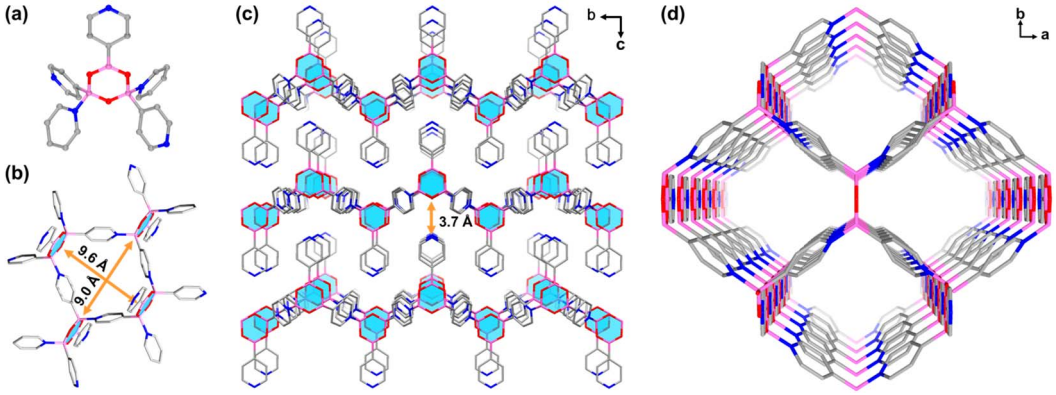

Fig. 1 (a) Connection mode of boroxine in BNOF-1. (b) Fragment of the tetrameric ring in BNOF-1. (c) 2D layers in BNOF-1 stacked along the *a*-axis. (d) The 3D supramolecular framework of BNOF-1 is viewed along the *c* axis. C gray, N navy, B pink, O red (H atoms are omitted for clarity).

(Fig. S1†). Thermogravimetric analysis (TGA) of BNOF-1 showed a 23.7% weight loss between 30 and 260 °C, and then a platform was displayed at 260–380 °C (Fig. S2†), demonstrating high thermal stability. Although BNOF-1 exhibits thermostability at high temperatures, it quickly decomposed into the monomer PBA in water and acidic/basic solutions (Fig. S3†), resulting from the nature of the boroxine formation as a reversible dehydration process.[42] The decomposition product, PBA, can be reused to synthesize BNOF-1 (Fig. S3†). However, BNOF-1 can retain its crystallinity in common organic solvents, such as EtOH, CH_2Cl_2, MeCN, *n*-hexane, *N*,*N*-dimethylformamide, methylbenzene (MB), and acetone (Fig. S4†).

Large-scale production and regeneration

Notably, the highly crystalline BNOF-1 material can be facily synthesized with gram-scale and a high yield, which is imperative from a view of industrial application. In a laboratory attempt, 0.73 g of BNOF-1 could be produced from 1 g of PBA by simply improving the raw material amount (Fig. 2a). Interestingly, the crystals of BNOF-1 can be dissolved in a hot organic solution, and the high-quality crystalline samples can be obtained again by slowly evaporating (Fig. 2b). This process is predominant due to the good reversibility of B←N bonds that enables recrystallization to the original framework after breakage and reassembly,[38,44] indicating the excellent regenerability and solution processability of BNOF-1. The measured PXRD results are also consistent with the as-synthesized pattern, indicating phase purity (Fig. S1†).

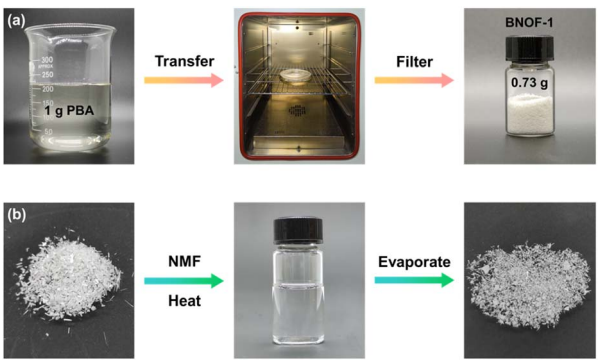

Fig. 2 (a) Large-scale synthesis and (b) regeneration process of BNOF-1.

Gas adsorption

Guest-free BNOF-1 can be readily produced by heating under a vacuum at 433 K for 10 h, where BNOF-1 maintains crystallinity after activation (Fig. S1†). The activated sample does not contain guest molecules, as confirmed by TGA (Fig. S2†). The permanent porosity of BNOF-1 was proven by N_2 adsorption at 77 K. At low pressure (P/P_0 < 0.01), the adsorption amount increased rapidly, exhibiting the I-type adsorption curve of microporous materials with a saturated loading of 340.7 $cm^3\ g^{-1}$ (Fig. 3a). By fitting the adsorption data, Brunauer–Emmett–Teller (BET) and Langmuir specific surface areas were 1345 and 1450 $m^2\ g^{-1}$, respectively. BNOF-1 represents the highest BET surface areas reported for B–N-based compounds (≤314 $m^2\ g^{-1}$) to date.[44] According to the Horvath–Kawazoe (H–K) model, the pore size of BNOF-1 is approximately 4.5–9.0 Å (Fig. 3a inset), which is close to the pore aperture metrics from the structure. The experimental pore volume of BNOF-1 is ~0.50 $cm^3\ g^{-1}$ (P/P_0 = 0.12), agreeing with the theoretical pore volume (0.55 $cm^3\ g^{-1}$). Furthermore, the porosity and BET surface areas can be well maintained for the scale-up and regenerated crystals (Fig. 3f and S5†).

C_2H_2 is an important raw material widely used in the production of chemical products.[53] In industry, trace CO_2 is inevitably mixed in the process of producing C_2H_2 through partial combustion of methane or steam cracking,[54] which seriously affects the purity of C_2H_2 in applications. However, as they have identical kinetic diameters (3.3 Å) and similar boiling points (C_2H_2, 189.3 K; CO_2, 194.7 K, Scheme S1†),[55,56] C_2H_2–CO_2 separation is extremely challenging. However, BNOFs have not been explored in the field of gas separation. Inspired by the high porosity and large specific surface area of BNOF-1, we further investigated the adsorption properties of C_2H_2 and CO_2. As shown in Fig. 3b, the adsorption capacities of C_2H_2 at 273 and

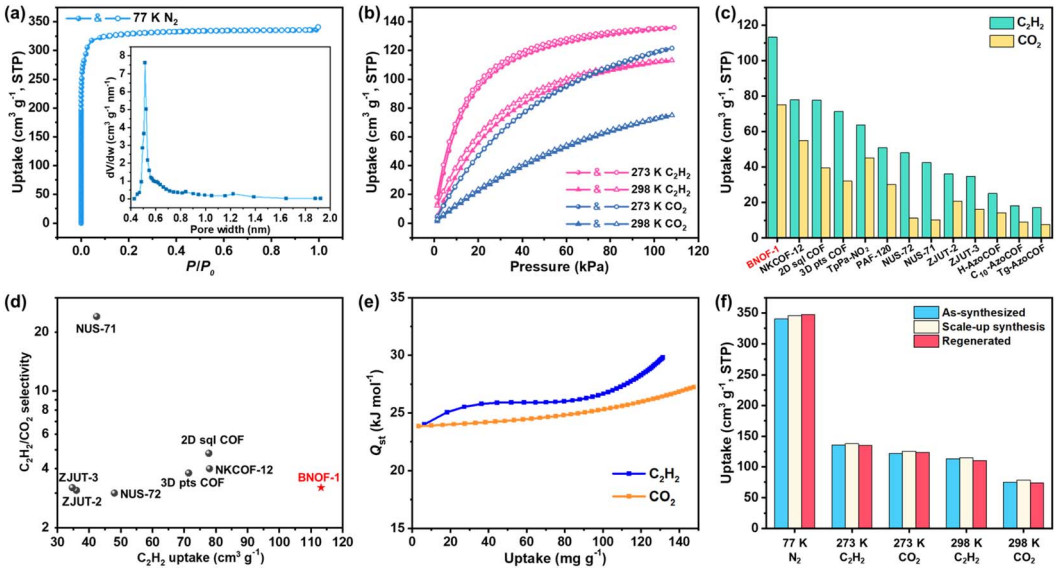

Fig. 3 (a) N_2 sorption isotherm and pore size distribution of BNOF-1 at 77 K. (b) C_2H_2 and CO_2 sorption isotherms of BNOF-1 at 273 and 298 K. (c) Comparison of C_2H_2 and CO_2 uptakes by BNOF-1 with other C_2H_2-selective COF materials at 298 K. (d) Comparison of selectivity and C_2H_2 adsorption uptake among COFs at 298 K and 100 kPa. (e) Q_{st} of BNOF-1 for C_2H_2 and CO_2. (f) Comparison of adsorption amounts for N_2, C_2H_2, and CO_2 in different samples of BNOF-1.

298 K at 1 bar are 135.9 and 113.2 $cm^3\ g^{-1}$, respectively. The corresponding uptakes of CO_2 are 121.6 and 75.2 $cm^3\ g^{-1}$, respectively. From the crystal density and uptake, the C_2H_2 storage density in BNOF-1 at 298 K was calculated to be 1.48 g cm^{-3}, which is far beyond the safe compression limit at 2 bar (~704 times, 0.0021 g cm^{-3}).[57] In addition, the uptake amounts of BNOF-1 for large-scale prepared and regenerated samples remain unchanged, demonstrating the feasibility of large-scale synthesis and the intactness of the restored framework (Fig. 3f and S6–S9†). Under ambient conditions, BNOF-1 exhibits the highest volumetric adsorption capacity for C_2H_2 and CO_2 (113.2, 75.2 $cm^3\ g^{-1}$) as compared to the reported COF materials, such as NKCOF-12 (78, 55 $cm^3\ g^{-1}$),[58] 2D sql COF (77.8, 39.4 $cm^3\ g^{-1}$),[59] 3D pts COF (71.4, 32 $cm^3\ g^{-1}$),[59] TpPa-NO_2 (63.73, 45.18 $cm^3\ g^{-1}$),[60] PAF-120 (50.8, 30 $cm^3\ g^{-1}$),[61] NUS-72 (48, 11.2 $cm^3\ g^{-1}$),[62] NUS-71 (42.4, 10.3 $cm^3\ g^{-1}$),[62] ZJUT-2 (36, 20.7 $cm^3\ g^{-1}$),[63] ZJUT-3 (34.7, 16.1 $cm^3\ g^{-1}$),[63] *et al.* (Fig. 3c and Table S1†), which could be a new benchmark organic framework for C_2H_2 and CO_2 storage.

Gas selectivity

Given the significant C_2H_2 loading of BNOF-1, the ideal adsorbed solution theory (IAST) was used to evaluate the separation performance of BNOF-1 on C_2H_2 and CO_2 mixtures. According to the fitting results through the single-point Langmuir–Freundlich equation (Fig. S10†), the selectivity of 2.8–3.2 at 298 K (Fig. S11†) is comparable to other COFs, such as ZJUT-2 (3.2),[63] 2D sql COF (4.8),[59] and NKCOF-12 (5.8)[58] (Fig. 3d). Subsequently, the Virial II equation was used to estimate the interactions of BNOF-1 with C_2H_2 and CO_2 (Fig. S12†). As shown in Fig. 3e, the adsorption heats (Q_{st}) of CO_2 and C_2H_2 at 298 K were in the range of 23.8–27.3 and 24.0–29.8 kJ mol^{-1}, respectively. The Q_{st} for both C_2H_2 and CO_2 increased with the uptake, which may be because the adsorption process benefits from molecular interactions between the adsorbates.[64,65] The overall higher Q_{st} of BNOF-1 for C_2H_2 than CO_2, indicates a higher affinity. The zero-loading Q_{st} (24.0 kJ mol^{-1}) of BNOF-1 for C_2H_2 is lower than some known COFs (Table S1†). Such a moderate Q_{st} implies that the regeneration of BNOF-1 material is more energy-saving for the uptake and release of C_2H_2.

Molecular simulations

To accurately illustrate the interactions between BNOF-1 and gas molecules, the preferential combined sites of C_2H_2 and CO_2

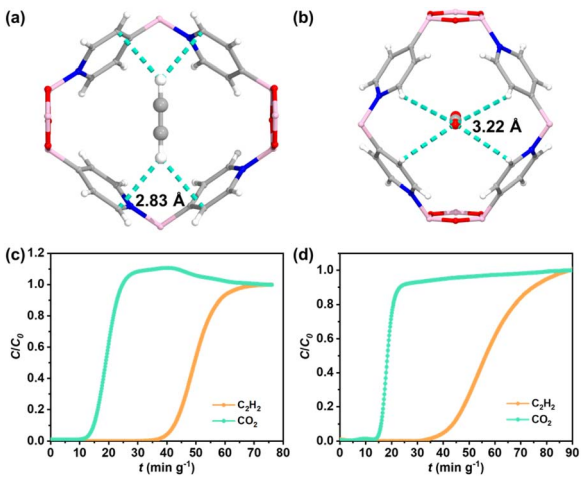

Fig. 4 Preferential adsorption sites for (a) C_2H_2 and (b) CO_2. Breakthrough plots for the separation of C_2H_2/CO_2 mixtures at 298 K: (c) C_2H_2–CO_2–Ar = 5%–5%–90%, (d) C_2H_2–CO_2–Ar = 5%–10%–85%.

in the framework were simulated by using the Grand Canonical Monte Carlo (GCMC). As described in Fig. 4a and b, both CO_2 and C_2H_2 molecules are located in the centre of the rhombic channel of BNOF-1. The adsorbed CO_2 molecule shows a side-on orientation, while C_2H_2 has an end-on orientation in terms of the local pore environment, which has also been observed in previous reports on energy reduction.[66] One O atom of CO_2 molecule forms four C–H···O hydrogen bonds (~3.22 Å) with the C–H units of four pyridine rings. For the C_2H_2 molecule, two H atoms form four C–H···C hydrogen bonds with the C atoms of four pyridine rings (~2.83 Å), as reported in other MOF materials.[67] These similar weak interactions explain the small difference in Q_{st} between C_2H_2 and CO_2, but as the hydrogen bonds formed by the framework with C_2H_2 are shorter than CO_2, it leads to stronger interactions for C_2H_2 from the framework.

Breakthrough experiment

To verify the ability of BNOF-1 to capture C_2H_2 and separate C_2H_2/CO_2 in gas mixtures, the activated BNOF-1 (0.6 g) was filled into the packed bed for dynamic breakthrough experiments. At a flow rate of 5 mL min^{-1}, CO_2 was detected at 15 min g^{-1} for the equimolar C_2H_2 and CO_2 mixture (C_2H_2–CO_2–Ar = 5%–5%–90%), while C_2H_2 could be retained at 40.4 min g^{-1}. Therefore, the penetration time interval was 25.3 min g^{-1} (Fig. 4c), exceeding COF material NKCOF-12 (14 min g^{-1})[58] and MOF material FJU-22 (11 min g^{-1})[68] under similar conditions. Based on the working capacity, 1 kg of BNOF-1 could adsorb 12.5 L of C_2H_2 in BNOF-1 and directly produce 4.0 L of CO_2 with high purity (>99.0%). The yield of C_2H_2 was higher than that of NKCOF-12 (10.04 L),[58] but lower than the COF materials, NUS-71 (31.4 L)[62] and NUS-72 (35.8 L),[62] as well as several benchmark MOFs for C_2H_2/CO_2 separation supported by open metal sites and/or polar functional groups, such as TIFSIX-2-Cu-i (73.9 L),[69] FJU-90 (41.9 L),[70] CPL-1-NH_2 (30.9 L),[71] and UTSA-300 (17.2 L).[72] The dynamic separation ratio could be determined to be 3.1, which was consistent with the IAST selectivity (3.2) and surpassed the values in some MOFs, such as FJU-22 (1.9),[68] SNNU-45 (2.9),[73] and NKMOF-1-Ni (2.6).[74] When the ratio of C_2H_2 and CO_2 is changed to 1 : 2 (C_2H_2–CO_2–Ar = 5%–10%–85%), BNOF-1 can still completely separate C_2H_2 and CO_2, with the breakthrough time interval of 25 min g^{-1} (Fig. 4d). The excellent C_2H_2/CO_2 separation ability of BNOF-1 may be attributed to high C_2H_2 adsorption capacity and significant C_2H_2/CO_2 selectivity. In addition, after the breakthrough experiments, the samples of BNOF-1 are still intact, as confirmed by PXRD (Fig. S1†).

Conclusions

In conclusion, we present the first example of crystalline microporous 2D BNOF with permanent porosity, which was constructed through single-component monomers. BNOF-1 with high porosity shows the highest surface area amongst known BNOFs and a benchmark C_2H_2 adsorption capacity in COFs. BNOF-1 can be conveniently prepared on a large scale by a one-step reaction and regenerated under mild conditions. The breakthrough experiment proves that BNOF-1 can efficiently separate CO_2 and C_2H_2 mixtures with a long C_2H_2 retention time and high dynamic selectivity. The synthesis of BNOF-1 would enrich supramolecular chemistry and reticular chemistry. It is expected that more innovative B←N bonds-based organic frameworks will be produced for their broad applications in the future. Notably, a newly published study reported an example of BNOF with permanent porosity during the peer review stage of this study, which was based on two different monomers with a relatively low surface area (255 m^2 g^{-1}) compared to BNOF-1.[75]

Data availability

All experimental supporting data are provided in the ESI.†

Author contributions

W. Wang and L. Wang conceived the idea and designed the project, and they contributed equally to this work. L. Wang, F. Du and G.-D. Wang worked on the synthesis and characterization. W. Wang, B. Liu, and L. Hou analyzed the results and wrote the manuscript. B. Liu, L. Hou, Y.-Y. Wang, and Z. Zhu provided reagents, materials, and analysis tools, as well as supervised the work. All authors contributed to the discussion and revised the manuscript.

Conflicts of interest

There are no conflicts to declare.

Acknowledgements

The authors acknowledge the support of this work by the Natural Science Foundation of Shaanxi Province (2021JM-084), and the National Natural Science Foundation of China (21871220).

Notes and references

1 M. E. Davis, C. Saldarriaga, C. Montes, J. Garces and C. Crowdert, *Nature*, 1988, **331**, 698–699.
2 C. T. Kresge, M. E. Leonowicz, W. J. Roth, J. C. Vartuli and J. S. Beck, *Nature*, 1992, **359**, 710–712.
3 M. E. Davis, *Nature*, 2002, **417**, 813–821.
4 H. Furukawa, K. E. Cordova, M. O'Keeffe and O. M. Yaghi, *Science*, 2013, **341**, 1230444.
5 A. J. Howarth, Y. Liu, P. Li, Z. Li, T. C. Wang, J. T. Hupp and O. K. Farha, *Nat. Rev. Mater.*, 2016, **1**, 15018.
6 G. Maurin, C. Serre, A. Cooper and G. Férey, *Chem. Soc. Rev.*, 2017, **46**, 3104–3107.
7 A. P. Côté, A. I. Benin, N. W. Ockwig, M. O'Keeffe, A. J. Matzger and O. M. Yaghi, *Science*, 2005, **310**, 1166–1170.
8 S.-Y. Ding and W. Wang, *Chem. Soc. Rev.*, 2013, **42**, 548–568.

9 K. Geng, T. He, R. Liu, S. Dalapati, K. T. Tan, Z. Li, S. Tao, Y. Gong, Q. Jiang and D. Jiang, *Chem. Rev.*, 2020, **120**, 8814–8933.
10 S. Yuan, J.-S. Qin, C. T. Lollar and H.-C. Zhou, *ACS Cent. Sci.*, 2018, **4**, 440–450.
11 X. Li, S. Cai, B. Sun, C. Yang, J. Zhang and Y. Liu, *Matter*, 2020, **3**, 1507–1540.
12 K. Liu, Y. Kang, Z. Wang and X. Zhang, *Adv. Mater.*, 2013, **25**, 5530–5548.
13 A. G. Slater and A. I. Cooper, *Science*, 2015, **348**, aaa8075.
14 K. T. Mahmudov, M. N. Kopylovich, M. F. C. Guedes da Silva and A. J. L. Pombeiro, *Coord. Chem. Rev.*, 2017, **345**, 54–72.
15 C. B. Aakeröy and K. R. Seddon, *Chem. Soc. Rev.*, 1993, **22**, 397–407.
16 S. Subramanian and M. J. Zaworotko, *Coord. Chem. Rev.*, 1994, **137**, 357–401.
17 G. Berger, J. Soubhye and F. Meyer, *Polym. Chem.*, 2015, **6**, 3559–3580.
18 B. Li, S.-Q. Zang, L.-Y. Wang and T. C. W. Mak, *Coord. Chem. Rev.*, 2016, **308**, 1–21.
19 Z.-F. Yao, J.-Y. Wang and J. Pei, *Cryst. Growth Des.*, 2018, **18**, 7–15.
20 L. J. Barbour, *Chem. Commun.*, 2006, 1163–1168.
21 T. Adachi and M. D. Ward, *Acc. Chem. Res.*, 2016, **49**, 2669–2679.
22 X. Zhang, Z. Chen, X. Liu, S. L. Hanna, X. Wang, R. Taheri-Ledari, A. Maleki, P. Li and O. K. Farha, *Chem. Soc. Rev.*, 2020, **49**, 7406–7427.
23 B. Wang, R.-B. Lin, Z. Zhang, S. Xiang and B. Chen, *J. Am. Chem. Soc.*, 2020, **142**, 14399–14416.
24 R.-B. Lin, Y. He, P. Li, H. Wang, W. Zhou and B. Chen, *Chem. Soc. Rev.*, 2019, **48**, 1362–1389.
25 X. Song, Y. Wang, C. Wang, D. Wang, G. Zhuang, K. O. Kirlikovali, P. Li and O. K. Farha, *J. Am. Chem. Soc.*, 2022, **144**, 10663–10687.
26 P. Silva, S. M. F. Vilela, J. P. C. Tomé and F. A. Almeida Paz, *Chem. Soc. Rev.*, 2015, **44**, 6774–6803.
27 M. Rubio-Martinez, C. Avci-Camur, A. W. Thornton, I. Imaz, D. Maspoch and M. R. Hill, *Chem. Soc. Rev.*, 2017, **46**, 3453–3480.
28 U. Ryu, S. Jee, P. C. Rao, J. Shin, C. Ko, M. Yoon, K. S. Park and K. M. Choi, *Coord. Chem. Rev.*, 2021, **426**, 213544.
29 L. Hashemi, M. Y. Masoomi and H. Garcia, *Coord. Chem. Rev.*, 2022, **472**, 214776.
30 Z. Liu and T. B. Marder, *Angew. Chem., Int. Ed.*, 2008, **47**, 242–244.
31 D. Salazar-Mendoza, J. Guerrero-Alvarez and H. Höpfl, *Chem. Commun.*, 2008, 6543–6545.
32 A. Dhara and F. Beuerle, *Chem.–Eur. J.*, 2015, **21**, 17391–17396.
33 R. Nishiyabu, Y. Kubo, T. D. James and J. S. Fossey, *Chem. Commun.*, 2011, **47**, 1124–1150.
34 K. Ono, S. Shimo, K. Takahashi, N. Yasuda, H. Uekusa and N. Iwasawa, *Angew. Chem., Int. Ed.*, 2018, **57**, 3113–3117.
35 E. C. Vargas-Olvera, F. J. Salas-Sánchez, A. Colin-Molina, S. Pérez-Estrada, B. Rodríguez-Molina, J. Alejandre, G. Campillo-Alvarado, L. R. MacGillivray and H. Höpfl, *Cryst. Growth Des.*, 2022, **22**, 570–584.
36 E. Sheepwash, V. Krampl, R. Scopelliti, O. Sereda, A. Neels and K. Severin, *Angew. Chem., Int. Ed.*, 2011, **50**, 3034–3037.
37 K. Severin, *Dalton Trans.*, 2009, 5254–5264.
38 B. Icli, E. Sheepwash, T. Riis-Johannessen, K. Schenk, Y. Filinchuk, R. Scopelliti and K. Severin, *Chem. Sci.*, 2011, **2**, 1719–1721.
39 N. Luisier, K. Bally, R. Scopelliti, F. T. Fadaei, K. Schenk, P. Pattison, E. Solari and K. Severin, *Cryst. Growth Des.*, 2016, **16**, 6600–6604.
40 Y. Kubo, R. Nishiyabu and T. D. James, *Chem. Commun.*, 2015, **51**, 2005–2020.
41 D. Kim, D. H. Jung, K.-H. Kim, H. Guk, S. S. Han, K. Choi and S.-H. Choi, *J. Phys. Chem. C*, 2012, **116**, 1479–1484.
42 Y. Du, K. Mao, P. Kamakoti, P. Ravikovitch, C. Paur, S. Cundy, Q. Li and D. Calabro, *Chem. Commun.*, 2012, **48**, 4606–4608.
43 A. P. Bapat, B. S. Sumerlin and A. Sutti, *Mater. Horiz.*, 2020, **7**, 694–714.
44 A. J. Stephens, R. Scopelliti, F. F. Tirani, E. Solari and K. Severin, *ACS Mater. Lett.*, 2019, **1**, 3–7.
45 H. Höpfl, *J. Organomet. Chem.*, 1999, **581**, 129–149.
46 A. L. Korich and P. M. Iovine, *Dalton Trans.*, 2010, **39**, 1423–1431.
47 G. Campillo-Alvarado, K. P. D'mello, D. C. Swenson, S. V. Santhana Mariappan, H. Höpfl, H. Morales-Rojas and L. R. MacGillivray, *Angew. Chem., Int. Ed.*, 2019, **58**, 5413–5416.
48 B. Icli, E. Solari, B. Kilbas, R. Scopelliti and K. Severin, *Chem.–Eur. J.*, 2012, **18**, 14867–14874.
49 J. Cruz-Huerta, D. Salazar-Mendoza, J. Hernández-Paredes, I. F. Hernández Ahuactzi and H. Höpfl, *Chem. Commun.*, 2012, **48**, 4241–4243.
50 D. Salazar-Mendoza, J. Cruz-Huerta, H. Höpfl, I. F. Hernández-Ahuactzi and M. Sanchez, *Cryst. Growth Des.*, 2013, **13**, 2441–2454.
51 C. Bao, Y.-J. Jiang, H. Zhang, X. Lu and J. Sun, *Adv. Funct. Mater.*, 2018, **28**, 1800560.
52 A. Torres-Huerta, M. J. Velásquez-Hernández, D. Martínez-Otero, H. Höpfl and V. Jancik, *Cryst. Growth Des.*, 2017, **17**, 2438–2452.
53 P. J. Stang and F. Diederich, *Modern Acetylene Chemistry*, VCH-Weinheim, 1995, pp. 1–499.
54 A. Corma, E. Corresa, Y. Mathieu, L. Sauvanaud, S. Al-Bogami, M. S. Al-Ghrami and A. Bourane, *Catal. Sci. Technol.*, 2017, **7**, 12–46.
55 J.-R. Li, R. J. Kuppler and H.-C. Zhou, *Chem. Soc. Rev.*, 2009, **38**, 1477–1504.
56 C. R. Reid and K. M. Thomas, *J. Phys. Chem. B*, 2001, **105**, 10619–10629.
57 W. Gong, H. Cui, Y. Xie, Y. Li, X. Tang, Y. Liu, Y. Cui and B. Chen, *J. Am. Chem. Soc.*, 2021, **143**, 14869–14876.
58 P. Zhang, Z. Wang, Y. Yang, S. Wang, T. Wang, J. Liu, P. Cheng, Y. Chen and Z. Zhang, *Sci. China Chem.*, 2022, **65**, 1173–1184.

59 L. Chen, C. Gong, X. Wang, F. Dai, M. Huang, X. Wu, C.-Z. Lu and Y. Peng, *J. Am. Chem. Soc.*, 2021, **143**, 10243–10249.
60 X.-H. Xiong, L. Zhang, W. Wang, N.-X. Zhu, L.-Z. Qin, H.-F. Huang, L.-L. Meng, Y.-Y. Xiong, M. Barboiu, D. Fenske, P. Hu and Z.-W. Wei, *ACS Appl. Mater. Interfaces*, 2022, **14**, 32105–32111.
61 L. Jiang, P. Wang, M. Li, P. Zhang, J. Li, J. Liu, Y. Ma, H. Ren and G. Zhu, *Chem.–Eur. J.*, 2019, **25**, 9045–9051.
62 Z. Zhang, C. Kang, S. B. Peh, D. Shi, F. Yang, Q. Liu and D. Zhao, *J. Am. Chem. Soc.*, 2022, **144**, 14992–14996.
63 C. Gong, H. Wang, G. Sheng, X. Wang, X. Xu, J. Wang, X. Miao, Y. Liu, Y. Zhang, F. Dai, L. Chen, N. Li, G. Xu, J. Jia, Y. Zhu and Y. Peng, *Angew. Chem., Int. Ed.*, 2022, **61**, e202204899.
64 S. Yang, A. J. Ramirez-Cuesta, R. Newby, V. Garcia-Sakai, P. Manuel, S. K. Callear, S. I. Campbell, C. C. Tang and M. Schröder, *Nat. Chem.*, 2015, **7**, 121–129.
65 H. Zeng, M. Xie, Y.-L. Huang, Y. Zhao, X.-J. Xie, J.-P. Bai, M.-Y. Wan, R. Krishna, W. Lu and D. Li, *Angew. Chem., Int. Ed.*, 2019, **58**, 8515–8519.
66 M. L. Foo, R. Matsuda, Y. Hijikata, R. Krishna, H. Sato, S. Horike, A. Hori, J. Duan, Y. Sato, Y. Kubota, M. Takata and S. Kitagawa, *J. Am. Chem. Soc.*, 2016, **138**, 3022–3030.
67 S.-Q. Yang, L. Zhou, Y. He, R. Krishna, Q. Zhang, Y.-F. An, B. Xing, Y.-H. Zhang and T.-L. Hu, *ACS Appl. Mater. Interfaces*, 2022, **14**, 33429–33437.
68 Z. Yao, Z. Zhang, L. Liu, Z. Li, W. Zhou, Y. Zhao, Y. Han, B. Chen, R. Krishna and S. Xiang, *Chem.–Eur. J.*, 2016, **22**, 5676–5683.
69 K.-J. Chen, H. S. Scott, D. G. Madden, T. Pham, A. Kumar, A. Bajpai, M. Lusi, K. A. Forrest, B. Space, J. J. Perry and M. J. Zaworotko, *Chem*, 2016, **1**, 753–765.
70 Y. Ye, Z. Ma, R.-B. Lin, R. Krishna, W. Zhou, Q. Lin, Z. Zhang, S. Xiang and B. Chen, *J. Am. Chem. Soc.*, 2019, **141**, 4130–4136.
71 L. Yang, L. Yan, Y. Wang, Z. Liu, J. He, Q. Fu, D. Liu, X. Gu, P. Dai, L. Li and X. Zhao, *Angew. Chem., Int. Ed.*, 2021, **60**, 4570–4574.
72 R.-B. Lin, L. Li, H. Wu, H. Arman, B. Li, R.-G. Lin, W. Zhou and B. Chen, *J. Am. Chem. Soc.*, 2017, **139**, 8022–8028.
73 Y.-P. Li, Y. Wang, Y.-Y. Xue, H.-P. Li, Q.-G. Zhai, S.-N. Li, Y.-C. Jiang, M.-C. Hu and X. Bu, *Angew. Chem., Int. Ed.*, 2019, **58**, 13590–13595.
74 Y.-L. Peng, T. Pham, P. Li, T. Wang, Y. Chen, K.-J. Chen, K. A. Forrest, B. Space, P. Cheng, M. J. Zaworotko and Z. Zhang, *Angew. Chem., Int. Ed.*, 2018, **57**, 10971–10975.
75 H. Zhang, Y. Li, L. Chen, Y. Yang, H. Lin, S. Xiang, B. Chen and Z. Zhang, *Chem*, 2022, DOI: **10.1016/j.chempr.2022.10.023**.